Modelling of Aggregated Operation of Power Modules in Low-Voltage DC-Grids

K. Rykov [1], L. Ott [2] , J.L. Duarte [1], E.A. Lomonova [1]
[1] EINDHOVEN UNIVERSITY OF TECHNOLOGY, [2] FRAUNHOFER IISB
Eindhoven University of Technology
P. O. Box 513, 5600MB
Eindhoven, The Netherlands
Phone: +31 (0) 40 247-3504
Email: k.rykov@tue.nl
URL: http://www.tue.nl/epe; http://www.dcc-g.eu

Acknowledgments

The paper was written based on research activities conducted within the ENIAC's project "Direct Current Components and Grid" (DCC+G).

Keywords

<<Microgrid>>, <<Renewable energy systems>>, <<Impedance measurement>>, <<Small-signal stability>>, <<Low-voltage DC-grids>>.

Abstract

The paper focuses on small-signal analysis of aggregated operation of the low-voltage DC-grids comprising various power and load modules. Complex impedances, which can be identified experimentally, represent the internal structure of power converters and may become a reason for voltage instabilities while being gathered together in the DC-grid using cables. The paper proposes ideas to analyze and forecast possible resonance issues of parallel operation of power modules in the test model of the 380V DC-grid and make recommendations in order to avoid them.

Introduction

Distributed generation using sustainable energy sources is aimed to become the main contributor in electricity production throughout the world in near future. Long-term damage to the environment caused by utilization of fossil fuels, such as coal, gas and oil, together with limited reserves and availability of those resources, put the ideas of effective use of green energy to be of paramount importance in modern society. Despite of the fact that the existing applications using hydrogen, geothermal, wind and solar types of power have been already contributing to the mentioned goal, significant steps should be taken to them accessible, flexible and easy deployable. Utilization of DC-microgrids is one of the promising examples of such steps [1-4].

Being complex systems, low-voltage DC-microgrids up to 1500 VDC include several modules (sources and loads), connected to the common bus with cables, with different power levels, control loops and EMC filters. Complexity of such systems is defined by the electrical impedances, representing the internal structure of separate modules and the whole system . Under certain conditions separately stable components of the grid may have voltage harmonics interaction issues, which in turn lead to unstable operation of the entire system. There have been studies done in stability analysis of DC systems [5,6]. Taking into account growing scale of the microgrids applications based on low-voltage DC current the problem of small-signal voltage instabilities becomes more and more topical. The possibility of analysis and forecasting those instabilities was presented and proved in [7,8]. Power converters were represented as average models using Norton equivalents and combined together with constant power loads into the grid containing limited number of modules. Change of control parameters of power modules, values of output capacitances and lengths of cables made it clear that the system response, based on bode plots

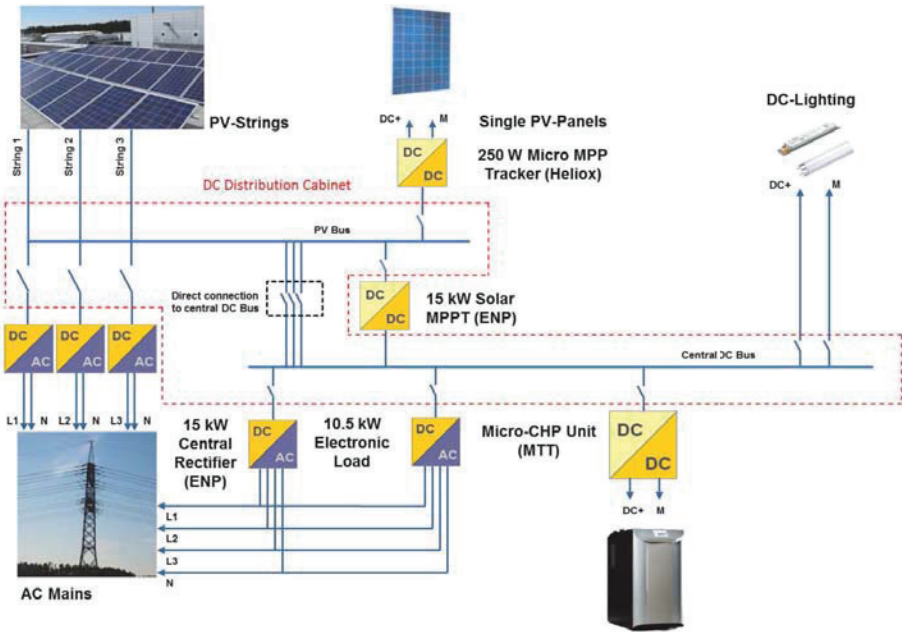

Figure 1: Aggregated DC test grid at Fraunhofer IISB.

and Nyquist diagrams analysis and time-domain simulations, could be unstable. It was also important to demonstrate that the internal structure of power modules in a form of complex impedance can be identified by the experimental identification approach described in [2], because in most of the cases this information is not available for end users. The method is based on injecting AC-excitation voltages from the specified frequency range with voltage and current measurements enabling for direct impedance calculation.

The paper contains small-signal analysis of the model of the real low-voltage (380 VDC) grid for an office building designed within the European Union project "Direct-Curent Components and Grid" (DCC+G) [9]. Description of the grid is followed by system aggregation, where parallel operation of several power modules (solar microconverter, AC-rectifier, micro combined heat and power unit converter, DC LED Driver, and programmable load) under different conditions is investigated with subsequent conclusions and comments about system stability.

Description of the DC-Grid Model

The main goal of the paper is to perform analysis of the aggregated operation of power modules in terms of small-signal voltage stability based on the 380 V DC test grid built at the Fraunhofer IISB Research Institute (Erlangen, Germany) within the DCC+G project. The sources and loads of the test grid interface the grid through power electronic components that were developed within the DCC+G project, such as the central rectifier (Emerson Network Power), the DC LED driver (Philips), the Solar Micro Inverter (Heliox) and the Micro-CHP unit (MTT), and through commercially available switch mode power supplies which were retrofitted for direct use in a 380 VDC grid environment, e. g. the fluorescent light drivers. A schematic build-up of the test-grid can be found in Fig. 1.

As can be seen from Fig. 1 the energy distribution inside the grid is realized radially originating from the so called DC Distribution Cabinet, a switchboard which contains all necessary circuit breakers, switches and controls to ensure a operation within a safe operation area and to interrupt the potential fault current. The switchboard itself contains two bus bars, the central DC bus and the photovoltaic (PV) bus. The difference between the two buses is that the voltage of the central DC bus is controlled to the nominal value of 380 VDC. The described droop control scheme in each power converter connected to this bus ensures keeping the voltage between 10 % boundaries of the nominal value. The PV bus on the other side has unregulated voltage which depends on the irradiation on the solar panels. The connection to the central DC for the PV panels can be realized in two ways. The first approach is to series connect a certain amount of PV panels and form a string. The maximum power point tracking (MPP) tracking for the whole string is then executed by a 15 kW DC/DC converter. Another possibility is to use panel integrated MPP trackers in the power range of 250 W. These power converters step up the panel voltage directly to the 380 VDC bus voltage and realize MPP tracking for each panel individually, which is superior to the string connection in case of clouding. Both possibilities for PV panel connection to the central DC bus are realized in the DC test grid.

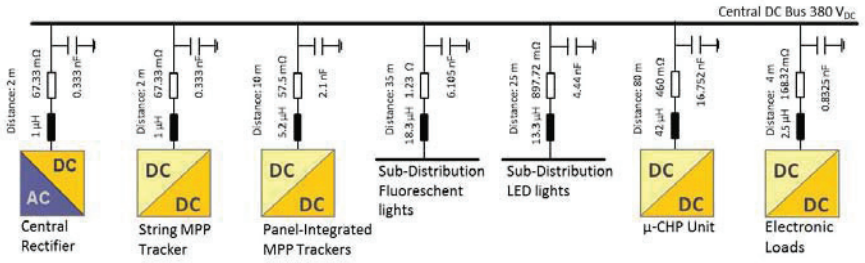

Figure 2: Main Power Modules of the DC Test Grid with specific connection impedance to the central DC bus.

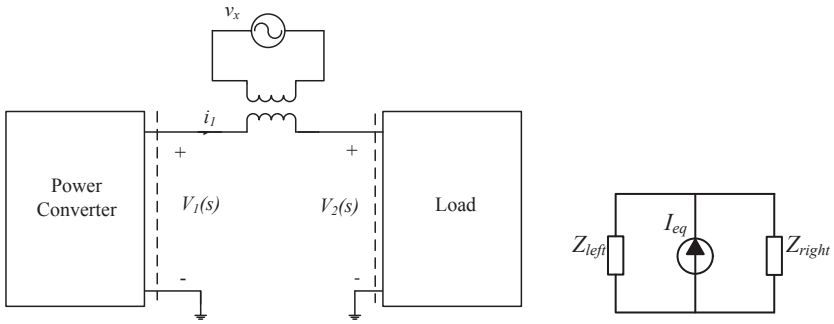

Figure 3: (a) Impedance identification method applied to a single converter (load) module; (b) Simplified impedance representation at one of the points of connection in the DC grid.

For all stability considerations the length of the cables that are used to connect sources and loads with their characteristic impedance per unit lengths are of great importance. The values for the RLC equivalent circuits were computed based on the impedance measurements done for each cable type with an impedance analyser. For example, the micro-CHP unit and the EV charger are connected to the central DC bus with a 4 G 6 cable type. For this type of cable, the following measurement values were obtained: L=0.525 H/m, R=5.75 m/m, C=0.21 nF/m.

Since all sources and loads are connected in a radial manner originating at the described DC distribution box, Fig. 2 shows the build-up of the DC grid with specific cable length and measured values for the equivalent RLC circuits. As can be seen in Fig. 2 the lighting grid consists of two parts. One part is built with fluorescent lights; the second is equipped with LED lights. This build-up was selected to enable a technology comparison in the context of DC grids. Both lighting grids are fed out of sub-distributions that are supplied out the central DC bus. Nevertheless, the stability analysis does only include two parallel LED distribution lighting grids, taking into account power load equal to the original set-up. The build-up of both sub-distribution systems was omitted here for simplicity.

Principle of the Voltage Stability Analysis

In order to apply voltage stability analysis, all power module impedances should be preliminarily assessed using experimental impedance identification approach [8]. The schematics depicted in Fig. 3 describes the principle of the approach. The wave generator injects amplified AC excitation voltages ($\approx$ 2VAC) of different frequencies into the line between the power module under investigation and load through the transformer. Being measured according to the convention of being fed into the grid, the introduced AC current together with voltage allow for obtaining impedance expressions

$$Z_1(s) = \frac{\| V_1(s) \|}{\| I_1(s) \|} [\angle V_1(s) + \angle I_1(s)] \qquad \text{and} \qquad Z_2(s) = \frac{\| V_2(s) \|}{\| I_1(s) \|} [\angle V_2(s) - \angle I_1(s)] \tag{1}$$

on the left and right side from excitation correspondingly. Impedance values in the specified frequency range result in a frequency response of a device. Frequency responses of five devices from the test DC grid including the 15kW central rectifier, the 250W solar microconverter, the 28W DC LED Driver, the Micro-CHP unit converter, and the electronic configurable load working in a constant power mode of 500W are depicted in Fig. 4.

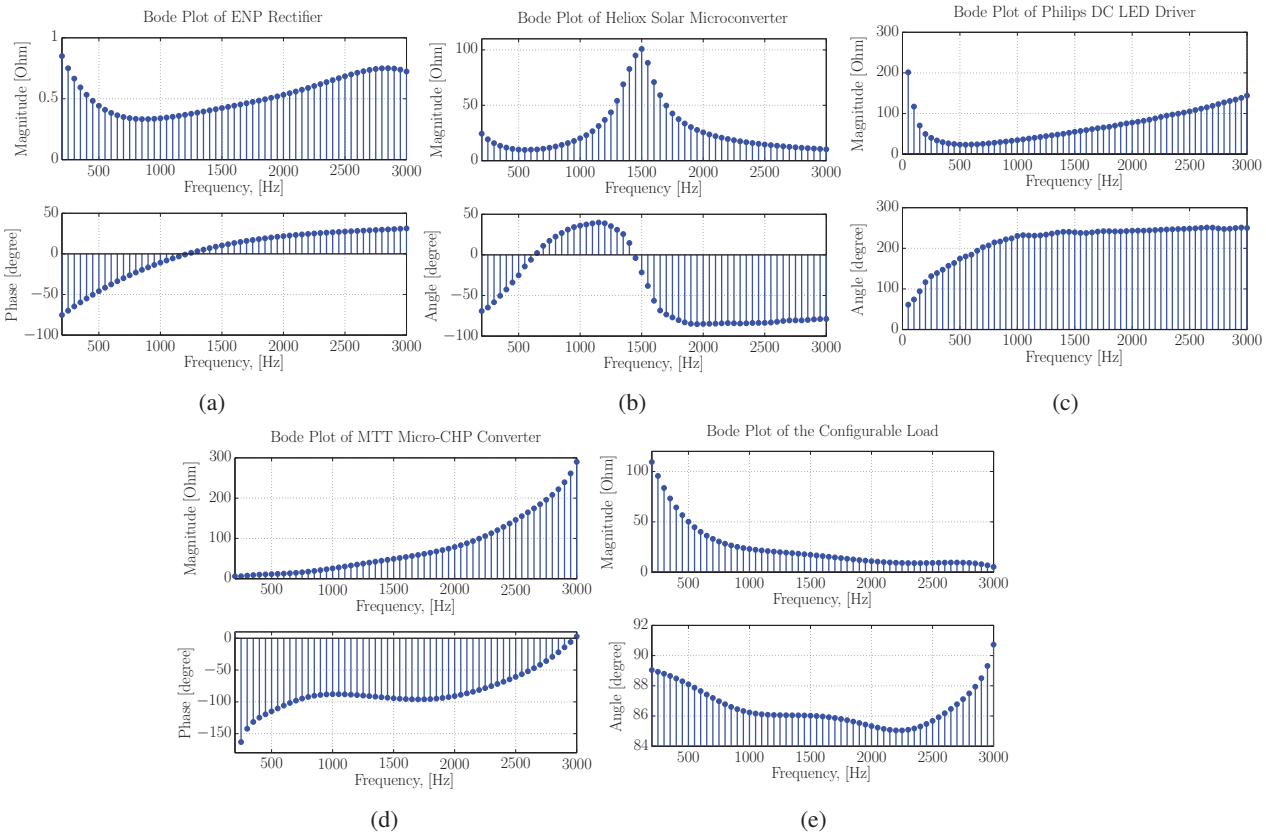

Figure 4: (a) Bode plot of the central rectifier; (b) Bode plot of the solar micro inverter; (c) Bode plot of the DC LED driver; (d) Bode plot of the Micro-CHP unit converter; (e) Bode plot of the configurable load.

System aggregation is based on building the admittance matrix [10], where the values, opposite to all identified impedances and impedances of connecting cables, are included, as explained in [8]. The resulting admittance matrix for the DC-grid consisting of N-modules

$$Y_{N,N} = \begin{bmatrix} Y_{11} & Y_{12} & \cdots & Y_{1N} \\ Y_{21} & Y_{22} & \cdots & Y_{2N} \\ \vdots & \vdots & \ddots & \vdots \\ Y_{k1} & Y_{k2} & \cdots & Y_{kN} \\ \vdots & \vdots & \ddots & \vdots \\ Y_{N1} & Y_{N2} & \cdots & Y_{NN} \end{bmatrix} \tag{2}$$

has the size of [N x N], where the elements of the main diagonal relate to admittances of the power modules themselves and adjacent elements correspond to admittances of cables interconnecting those modules.

Subsequently, the matrix is used for the analysis of the aggregated system. Considering any point of the grid (see Fig. 2) as a point of connection, for instance, at module k, the resulting matrix (2) should be divided into two parts – to the left and to the right from the point of connection with corresponding impedances $Z_{left} = 1/Y_{1,k(k,k)}$ and $Z_{right} = 1/Y_{k,N(1,1)}$. Resonance issues of two parallel impedances (Fig. 3(b)) occur when the denominator of the system transfer function $G(s) = 1/(1 + Z_{left}/Z_{right})$ equals to zero, in other words, the following condition $Z_{left}/Z_{right} = -1$, or $Z_{left} + Z_{right} = 0$ should be satisfied. In terms of amplitudes and phases of impedances Z_{left} and Z_{right} that means the amplitude components are equal and the phase shift is 180°. Frequencies, which correspond to these points of parallel resonance issues, give the basis for possible small-signal voltage instability problems, and allow for making assumptions to improve system stability by

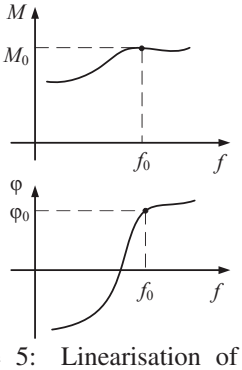

Figure 5: Linearisation of amplitude and phase components of impedance around frequency f_0.

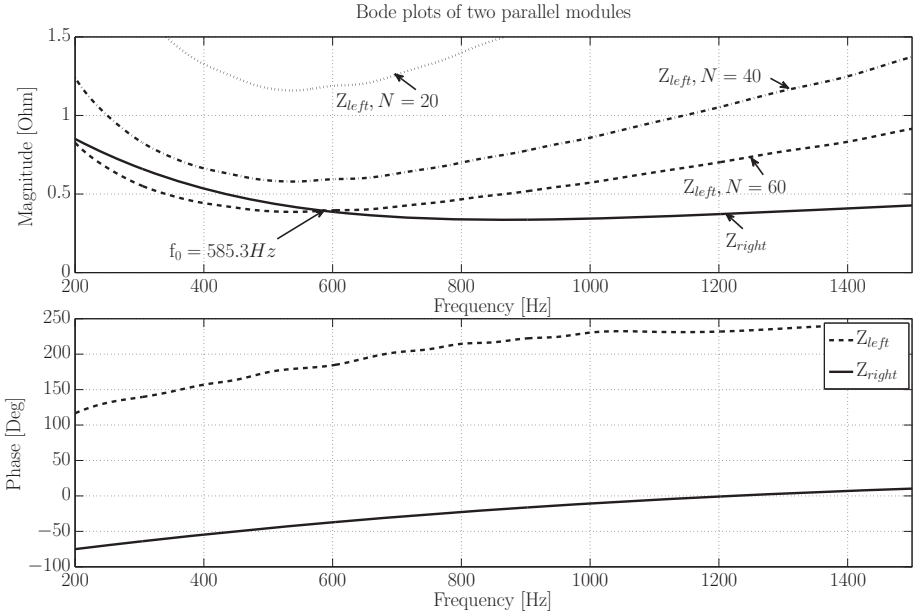

Figure 6: Bode plots of impedances Z_{right} and Z_{left} for $N_{\mathrm{LED}} = 20$, $N_{\mathrm{LED}} = 40$, and $N_{\mathrm{LED}} = 60$.

reconfiguring the grid using decreased number of items of the same type of modules working in parallel, shortening cable lengths, and introducing ballasts or filters. Practical implementation of the described technique is presented in details in the next section.

Parallel Operation of Two Modules

Let us investigate possible voltage stability issues considering parallel operation of two modules – 15 kW central rectifier, and one 28W DC LED driver interlinked by a short cable with negligible impedance value. It is important to be noticed that under the term voltage stability the paper relates to small-signal voltage stability at the specified frequency, corresponding harmonic of which may be introduced to the grid and cause the beginning of voltage oscillations. For the sake of analysis, complex impedances Z_{LED} and Z_{REC} of both modules (the LED driver and the rectifier) were linearised around the specified frequency f_0 (Fig. 5) taking into account that the amplitude is positive $M_0 > 0$ and the phase is located in the range $-180^\circ < \varphi_0 < 180^\circ$. Thus, making an assumption that in schematics in Fig. 3(b) $Z_{left} = Z_{\mathrm{REC}}$ and $Z_{right} = Z_{\mathrm{LED}}$, impedances of the left and right modules are expressed, as follows:

$$Z_{left,0} = M_{\mathrm{REC},0} \cdot \cos\varphi_{\mathrm{REC},0} + \mathrm{j} \cdot M_{\mathrm{REC},0} \cdot \sin\varphi_{\mathrm{REC},0} \tag{3}$$

$$Z_{right,0} = M_{\mathrm{LED},0} \cdot \cos\varphi_{\mathrm{LED},0} + \mathrm{j} \cdot M_{\mathrm{LED},0} \cdot \sin\varphi_{\mathrm{LED},0}. \tag{4}$$

The choice of frequency for linearisation should be based on analysis of combined bode plots of impedances Z_{left} and Z_{right}. The frequency ranges, where the load devices, such as the LED driver or the electronic load, demonstrate negative resistance behaviour, in other words, the real part of impedance $M_0 \cdot \cos\varphi_0 < 0$, deserve careful consideration. The condition $M_0 \cdot \cos\varphi_0 < 0$ is satisfied when $\cos\varphi_0 < 0$, thus $90^\circ < \varphi_0 < 270^\circ$. Consequently, from the identified area one should choose a point, where amplitudes are equal and resulting phase shift is 180°. Corresponding impedance related expressions are yielded from (3) and (4):

$$M_{\mathrm{REC},0} \cdot \cos\varphi_{\mathrm{REC},0} + M_{\mathrm{LED},0} \cdot \cos\varphi_{\mathrm{LED},0} = 0 \tag{5}$$

$$M_{\mathrm{REC},0} \cdot \sin\varphi_{\mathrm{REC},0} + M_{\mathrm{LED},0} \cdot \sin\varphi_{\mathrm{LED},0} = 0, \tag{6}$$

Visual comparison of bode plots of both the rectifier and the LED driver demonstrates that amplitude levels are significantly different in the whole frequency range. Moreover, there is no a single frequency that relates to the phase shift of 180°. It means, that conditions (5) and (6) cannot be met. Obviously, aggregated operation of the 15kW rectifier and the 28W LED lighting unit will not cause any stability problem. Nevertheless, there are ways to destabilize the system and, therefore, to investigate several stability scenarios. Let us consider two practical ways to shape parallel impedances in such a manner that the system starts to be unstable. Those two ways include changing a number of items of the specific

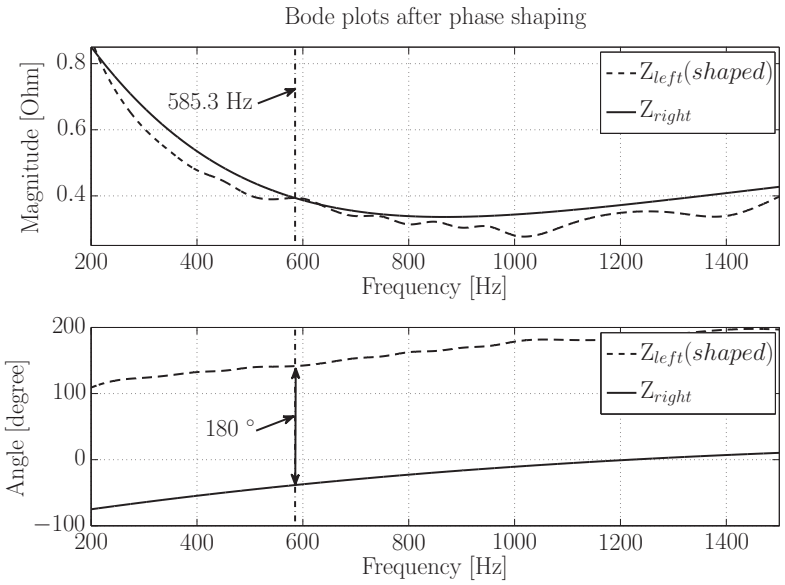

Figure 7: Bode plots of shaped impedances Z_{right} and Z_{left}.

module and varying cable lengths between modules. If the number of items is increased, the impedances Z_{left} and Z_{right} are changed appropriately, as follows:

$$Z_{left,0} = 1/N_{\mathrm{REC}} \cdot [M_{\mathrm{REC},0} \cdot \cos\varphi_{\mathrm{REC},0} + \mathrm{j} \cdot M_{\mathrm{REC},0} \cdot \sin\varphi_{\mathrm{REC},0}] \tag{7}$$

$$Z_{right,0} = 1/N_{\mathrm{LED}} \cdot [M_{\mathrm{LED},0} \cdot \cos\varphi_{\mathrm{LED},0} + \mathrm{j} \cdot M_{\mathrm{LED},0} \cdot \sin\varphi_{\mathrm{LED},0}], \tag{8}$$

where N_{REC} and N_{LED} are numbers of rectifier and LED modules respectively. Bode plots for one rectifier module as Z_{right} and three different numbers of LED modules ($N_{\mathrm{LED}} = 20$, $N_{\mathrm{LED}} = 40$, and $N_{\mathrm{LED}} = 60$) as Z_{left} are shown in Fig. 6. It can be concluded that increasing the number of LED modules from $N_{\mathrm{LED}} = 20$ to $N_{\mathrm{LED}} = 60$, which corresponds to the rise of power demand from 560W to 1680W, make the system closer to instabilities, since the first condition of equal amplitudes of Z_{left} and Z_{right} is satisfied for $N_{\mathrm{LED}} = 60$ at the frequency $f_0 = 585.3$Hz (Fig. 6). Nonetheless, phase components did not change, so the system in the described situation is still stable. Further analysis will be done for the number of rectifiers $N_{\mathrm{REC}} = 1$, the number of LEDs $N_{\mathrm{LED}} = 60$, and the frequency $f_0 = 585.3$Hz.

In scenarios when extra cable length between modules is introduced, the total impedance of one of the modules, for instance, the right one (rectifier module), is increased by the cable impedance $Z_c = R_c + \mathrm{j}\omega L_c$ ($\omega = 2\pi f_0$) and have the following expression:

$$\begin{aligned} Z_{right,tot} = Z_{left,0} + Z_c = R_c + \mathrm{j}\omega L_c + 1/N_{\mathrm{LED}} \cdot [M_{\mathrm{LED},0} \cdot \cos\varphi_{\mathrm{LED},0} + \mathrm{j} \cdot M_{\mathrm{LED},0} \cdot \sin\varphi_{\mathrm{LED},0}] = \\ = (R_c + 1/N_{\mathrm{LED}} \cdot M_{\mathrm{LED},0} \cdot \cos\varphi_{\mathrm{LED},0}) + \mathrm{j} \cdot (\omega L_c + 1/N_{\mathrm{LED}} \cdot M_{\mathrm{LED},0} \cdot \sin\varphi_{\mathrm{LED},0}). \end{aligned} \tag{9}$$

In contrast with changing the number of items, adding extra cable length causes both amplitude and phase changes of the module impedance. If the condition of parallel resonance $Z_{left} + Z_{right} = 0$ is rewritten using equations (7) and (9) separately for real and imaginary parts

$$\begin{cases} R_c + 1/N_{\mathrm{LED}} \cdot M_{\mathrm{LED},0} \cdot \cos\varphi_{\mathrm{LED},0} + 1/N_{\mathrm{REC}} \cdot M_{\mathrm{REC},0} \cdot \cos\varphi_{\mathrm{REC},0} = 0 \\ \omega L_c + 1/N_{\mathrm{LED}} \cdot M_{\mathrm{LED},0} \cdot \sin\varphi_{\mathrm{LED},0} + 1/N_{\mathrm{REC}} \cdot M_{\mathrm{REC},0} \cdot \sin\varphi_{\mathrm{REC},0} = 0 \end{cases} \tag{10}$$

the following equation

$$\begin{bmatrix} R_c \\ \omega L_c \end{bmatrix} = - \begin{bmatrix} M_{\mathrm{LED},0} \cdot \cos\varphi_{\mathrm{LED},0} & M_{\mathrm{REC},0} \cdot \cos\varphi_{\mathrm{REC},0} \\ M_{\mathrm{LED},0} \cdot \sin\varphi_{\mathrm{LED},0} & M_{\mathrm{REC},0} \cdot \sin\varphi_{\mathrm{REC},0} \end{bmatrix} \cdot \begin{bmatrix} 1/N_{\mathrm{LED}} \\ 1/N_{\mathrm{REC}} \end{bmatrix} \tag{11}$$

provides a possibility to calculate cable impedance components R_c and L_c, which will lead for the specified frequency f_0 to the resonance between two parallel modules Z_{REC} and Z_{LED}, consisting of N_{REC}

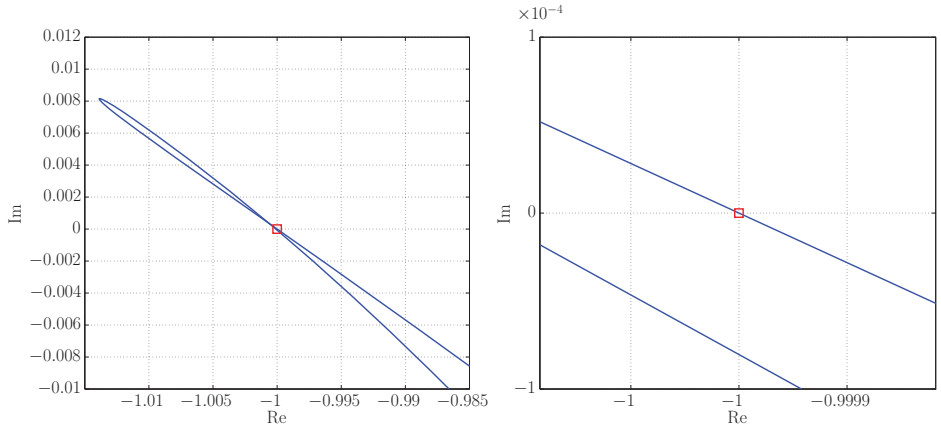

Figure 8: Nyquist plot of the system transfer function $G_s(s) = Z_{left}/Z_{right}$(left) and the zoomed view (right) it.

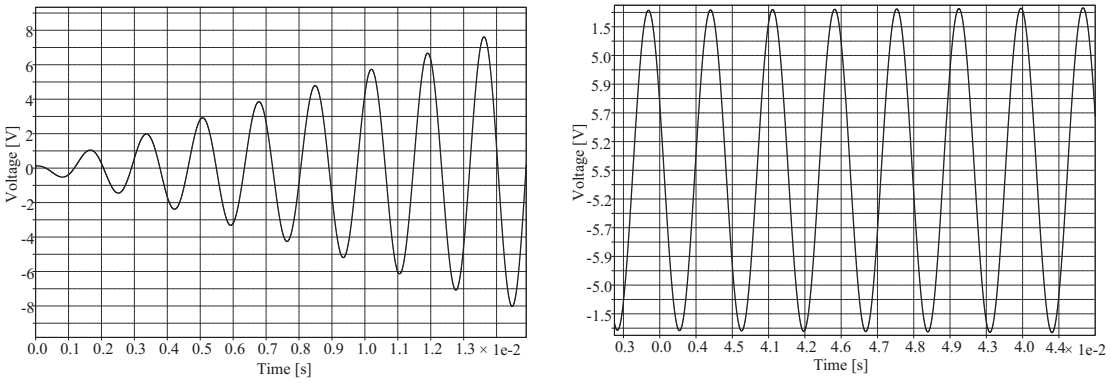

(a) (b)

Figure 9: (a) Unstable time-domain simulation of the linear model with parallel impedances; (b) Stable time-domain simulation of the linear model with parallel impedances.

and N_{LED} items correspondingly. For $N_{\text{REC}} = 1$, $N_{\text{LED}} = 60$, and $f_0 = 585.3$Hz, calculated cable resistance and inductance are equal to $R_c = 84.8\text{m}\Omega$ and $L_c = 71.37\mu$H respectively. Frequency responses of shaped impedances Z_{left} and Z_{right} are presented in Fig. 7. It is clear that at the frequency $f_0 = 585.3$Hz the amplitudes cross each other and the resulting phase shift is 180°.

Another way to confirm the fact of instability is to investigate a Nyquist plot (Fig. 8) using the system transfer function $G_s(s) = Z_{left}(s)/Z_{right}(s)$ [7]. The Nyquist plot crosses the point (-1;0) at the frequency f_0, which according to the Nyquist stability criterion indicates that the system is unstable. The fact of instability can be also observed from time-domain simulations in accordance with schematics in Fig. 3(b) representing the linearised model with two parallel impedances Z_{right} and Z_{left} shaped to achieve resonance at the specified frequency (Fig. 9(a)). It is clearly visible that the voltage oscillations have increasing amplitude, which indicates existence of parallel resonance issues. In contrast, for the same system but without additional cable length, voltage oscillations have a stable amplitude.

Analysis of a Complex Grid

Investigation of voltage instabilities based on parallel impedance interactions are also suitable for complex DC-grids. For the sake of validation of this statement, the 380V DC-grid developed within the DCC+G project at Fraunhofer IISB and described above, is considered. The model consists of six modules in correspondence with Fig. 2, which include the following components: the 15kW central rectifier, the 250W solar microconverter, the micro-CHP unit converter, two lighting sub-distribution systems consisting of 18 DC LED Drivers with total power of 504W each, and 21 items of electronic loads for office rooms providing total power demand of 10.5kW representing the separate system module. Bode plots of all devices were identified experimentally and have been already depicted in Fig. 4.

The system admittance matrix

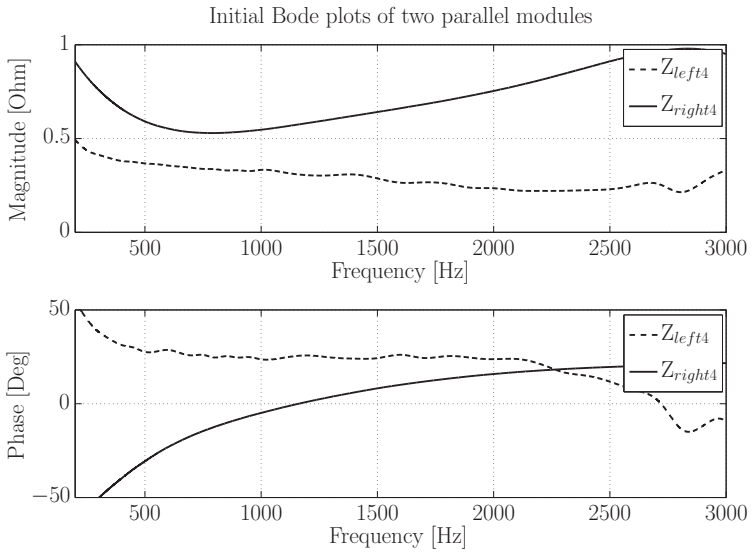

Figure 10: Combined view of parallel complex impedances Z_{left} and Z_{right}

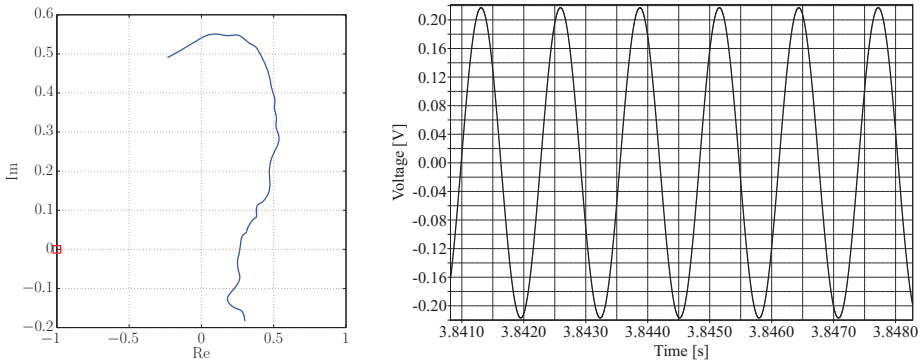

(a) (b)

Figure 11: (a) Nyquist plot of the stable grid; (b) Stable time-domain simulation of the linear model with parallel impedances.

$$Y_{6,6} = \begin{bmatrix} Y_{11} & Y_{12} & \cdots & Y_{16} \\ Y_{21} & Y_{22} & \cdots & Y_{26} \\ \vdots & \vdots & \ddots & \vdots \\ Y_{61} & Y_{62} & \cdots & Y_{66} \end{bmatrix} \tag{12}$$

of [6 x 6] size can be divided for the further analysis at one of the points of connection , for instance, at the module 4, into two parts with corresponding impedances Z_{left} and Z_{right}. Frequency responses presented in Fig. 10 demonstrate stable behaviour in the whole specified frequency range from 200Hz to 3000Hz, since amplitudes of parallel impedances do not cross each other and the phase shift is always less than 180°. Although both of complex impedances include parts corresponding to load modules, which separately may demonstrate negative resistance behaviour at certain frequencies, none of the impedances Z_{left} and Z_{right} have regions where phases are located in the $90° < \varphi_0 < 270°$ region.

Nevertheless, let us choose a frequency where the system could have instabilities under certain conditions. The frequency $f_0 = 780$Hz is closer than other points to satisfy instability conditions of equal amplitudes and resulting phase shift of 180°. Corresponding Nyquist plot, which doesn't cross the (-1;0) point (Fig. 11(a)) and time-domain simulation of the linear model of parallel impedances with the constant voltage amplitude (Fig. 11(b)) confirm the fact that the system is free of resonance issues at the specified frequency. Nonetheless, as it was demonstrated in the previous chapter, complex parallel impedances may react on system modifications by getting closer to resonance issues or even becoming unstable.

Conclusions

The reason for voltage instabilities in DC-grids is resonance issues caused by interaction of complex impedances, representing components of the grid. Different nature, structure, and power levels of grid modules, including sources and loads, interlinked with cables of various length and type make an impact on system behaviour. Presented approach gives the opportunity to analyse small-signal voltage stability at any point of the DC-grid and make conclusions with regard to different scenarios of operation.

References

[1] Ahmadi, R., Ferdowsi, M.: Modeling closed-loop input and output impedances of DC-DC power converters operating inside dc distribution systems, Applied Power Electronics Conference and Exposition (APEC), 2014 Twenty-Ninth Annual IEEE, pp. 1131 - 1138, Mar 2014.

[2] Poh, C., Blaabjerg, F.: Autonomous operation of hybrid microgrid with AC and DC sub-grids, Proceedings of the 2011-14th European Conference o nPower Electronics and Applications (EPE 2011), Aug-Sep 2011.

[3] Nasirian, V., Davoudi, A., Lewis, F.L.: Distributed adaptive droop control for DC microgrids, 2014 Twenty-Ninth Annual IEEE Applied Power Electronics Conference and Exposition (APEC), pp. 1147 - 1152, Mar 2014.

[4] Madduri, P.A., Rosa, J., Sanders, S.R., Brewer, E.A.: Design and verification of smart and scalable DC microgrids for emerging regions, 2013 IEEE Energy Conversion Congress and Exposition (ECCE), pp. 73 - 79, Sep 2013.

[5] Riccobono, A., Santi, E.: Comprehensive review of stability criteria for DC distribution systems, 2012 IEEE Energy Conversion Congress and Exposition (ECCE), pp. 3917 - 3925, Sep 2012.

[6] Riccobono, A., Siegers, J., Santi, E.: Stabilizing positive feed-forward control design for a DC power distribution system using a passivity-based stability criterion and system bus impedance identification, 2014 Twenty-Ninth Annual IEEE Applied Power Electronics Conference and Exposition (APEC), pp. 1139 - 1146, Mar 2014.

[7] Rykov, K., Duarte, J.L., Boeke, U., Wendt, M., Weiss, R.: Voltage stability assessment in semi-autonomous DC-grids with multiple power modules, 2013 15th European Conference on Power Electronics and Applications (EPE), pp. 1 - 10, Sep 2013.

[8] Rykov, K., Duarte, J.L., Szpek, M., Olsson, J., Zeltner, S., Ott, L.: Converter impedance characterization for stability analysis of low-voltage DC-grids, 2014 IEEE PES Innovative Smart Grid Technologies Conference (ISGT), pp. 1-5, Feb 2014.

[9] Eniac Joint Undertaking: DCC+G DC components and grid, Project Profile, 2011. Available: http://dcgrid.tue.nl/files/ENIAC-DCC+G_ project_ profile.pdf

[10] Wang, F, Duarte, J.L., Hendrix, M.A.M., Lomonova, E.A.,: Flexible operation of grid-interfacing converters in distribution networks: Ph.D. dissertation, Technische Universiteit Eindhoven pp. 1-10.